

Fulde-Ferrell superfluids in an asymmetric three-component Fermi Gas

Yuhan Lu,¹ Lihong Zhou,^{2,*} and Yongping Zhang^{1,†}

¹*Institute for Quantum Science and Technology, Department of Physics, Shanghai University, Shanghai 200444, China*

²*Institute for Quantum Science and Technology, Shanghai University, Shanghai 200444, China*

An asymmetric three-component Fermi gas, featuring Raman-induced spin-orbit coupling between the first and second components and contact interaction only between the first and third components, introduces both spin-orbit coupling and population imbalance-two mechanisms known to stabilize the Fulde-Ferrell superfluids. We systematically study Fulde-Ferrell superfluids in an asymmetric three-component Fermi gas by finding the global minima of the thermodynamic potential. We reveal a new class of composite Fulde-Ferrell superfluids that emerges when strong spin-orbit coupling generates a double-well structure in momentum space within the lower spin-orbit-coupled band. The key features of these composite superfluids are identified.

I. INTRODUCTION

The degenerate Fermi gases, experimentally realized in ultracold neutral atoms, provide a fundamental platform for investigating pairing superfluidity [1–3]. Owing to their parameter tunability, these systems also enable access to the unitary regime and the so-called BCS–BEC crossover [4–8].

Among exotic pairing superfluids in Fermi gases, Fulde-Ferrell (FF) pairs [9], characterized by an order parameter with a nonzero pairing momentum, and Larkin-Ovchinnikov (LO) pairs [10], featured by a spatially modulated order parameter, have attracted considerable research attention [11–14]. In a multiple-component Fermi gas, population imbalance induces a mismatch between the Fermi surfaces of different components [15–19]. Such Fermi surface mismatch arising from different energy bands has become an important mechanism for stabilizing FF superfluids [20–23]. With the experimental advancement of synthetic spin-orbit coupling (SOC) in ultracold atoms [24–26], SOC has been recognized as another mechanism for the emergence of FF pairs [27, 28]. The combination of SOC and an in-plane Zeeman field gives rise to an asymmetric Fermi surface with respect to the center of momentum within a single spin-orbit-coupled energy band. FF pairing occurs between states on this asymmetric surface. Meanwhile, SOC may also introduce topological properties to quasiparticles. Spin-orbit-coupled FF superfluids have been intensively investigated in two-component [29–42] and three-component [43–46] systems. Moreover, SOC brings new physics to the BCS-BEC crossover [47–51].

Ref. [52] proposed a new mechanism of FF pairing formation in an asymmetric three-component Fermi gas, which consists of SOC between the first and second components and contact interactions between the first and third components. This mechanism incorporates both SOC and population imbalance together and can generate two kinds of FF pairs originating from two spin-orbit-

coupled energy bands [52]. Since there is no conventional s-wave Cooper pair in this system, FF superfluids can exist in a broad parameter region.

In this paper, we systematically study FF superfluids in such the asymmetric three-component Fermi gas. The SOC, which exists only between the first and second components, causes these two components to share the same chemical potential μ_{12} and gives rise to two spin-orbit-coupled energy bands. In contrast, the third component, characterized by a chemical potential μ_3 , forms an isolated energy band. Due to the asymmetry of the interactions, pairing can only occur between the first and third components. If μ_{12} intersects with both spin-orbit-coupled energy bands, we identify two distinct types of FF superfluids, between which a first-order phase transition can be induced by varying μ_3 . On the other hand, if μ_{12} intersects only with the lower spin-orbit-coupled band, only one type of FF superfluid emerges. These findings are consistent with the results reported in Ref. [52].

If the SOC dominates, the lower spin-orbit-coupled band exhibits a double-well structure in momentum space. Letting μ_2 intersect this double-well structure can give rise to two states dominated by the first component. These two states combine to form a composite first-component state, whose average momentum corresponds to one of the minima of the double-well. Meanwhile, μ_3 intersects with the isolated band, generating the other composite state-dominated by the third component-with an average momentum of zero. Ultimately, these two composite states bind together to form a FF pair. The most notable feature of such a composite FF superfluid is that its pairing momentum remains invariant even when μ_{12} and μ_3 vary. This newly identified class of composite FF superfluids not only completes the study presented in Ref. [52], but also introduces a novel mechanism for the composite formation of FF pairs.

The rest of this paper is organized as follows. In Sec. II, we present the mean-field theoretical framework for the asymmetric three-component Fermi gas. In Sec. III, FF superfluids are investigated for the weak SOC case. In Sec. IV, we reveal a new composite FF superfluid for the strong SOC case. Finally, a conclusion is given in Sec. V.

* lihongzh@shu.edu.cn

† yongping11@t.shu.edu.cn

II. MODEL

We consider three-component Fermi gases confined in a quasi-two-dimension potential [52]. The system is described by the Hamiltonian,

$$H = \sum_{\mathbf{k}} \Phi^\dagger(\mathbf{k}) H_0(\mathbf{k}) \Phi(\mathbf{k}) + H_I, \quad (1)$$

where $\Phi(\mathbf{k}) = (c_{\mathbf{k},1}, c_{\mathbf{k},2}, c_{\mathbf{k},3})^T$ is the wave function with $c_{\mathbf{k},i}$ being annihilation operator in momentum space $\mathbf{k} = (k_x, k_y)$ for the i -th component. H_0 is the single-particle Hamiltonian in momentum space,

$$H_0(\mathbf{k}) = \begin{pmatrix} \varepsilon_{\mathbf{k}} - \mu_{12} + \alpha k_x & h & 0 \\ h & \varepsilon_{\mathbf{k}} - \mu_{12} - \alpha k_x & 0 \\ 0 & 0 & \varepsilon_{\mathbf{k}} - \mu_3 \end{pmatrix}. \quad (2)$$

Here,

$$\varepsilon_{\mathbf{k}} = \frac{\hbar^2 \mathbf{k}^2}{2m}, \quad (3)$$

is the single-particle kinetic energy with m being atom mass. The first and second components are resonantly coupled via a two-photon transition induced by a pair of Raman lasers [24, 25]. h is the two-photon coupling strength. Since the two Raman beams propagating oppositely in the x direction, the two-photon transition is accompanied by SOC with the strength α along the \hat{k}_x direction. The SOC manifests itself as the presence of $\pm\alpha k_x$ in the first and second component respectively. Furthermore, the Raman coupling gives rise to the same chemical potential μ_{12} to the first two components. While, the third component does not have a coupling with the previous ones, therefore, it has an independent chemical potential μ_3 . The interacting H_I in Eq. (1) describes the contact interaction between the first and third components,

$$H_I = \frac{U_{13}}{S} \sum_{\mathbf{q}, \mathbf{k}, \mathbf{k}'} \left(c_{\mathbf{k},3}^\dagger c_{\mathbf{q}-\mathbf{k},1}^\dagger c_{\mathbf{q}-\mathbf{k}',1} c_{\mathbf{k}',3} \right), \quad (4)$$

where U_{13} is the interaction rate and S is the area of two dimensional gas. The momentum conservation during collision generates three momenta $(\mathbf{k}, \mathbf{k}', \mathbf{q})$. The rate U_{13} in two-dimension can be renormalized as

$$\frac{S}{U_{13}} = - \sum_{\mathbf{k}} \frac{1}{2\varepsilon_{\mathbf{k}} + E_{b,13}}, \quad (5)$$

by introducing the binding energy $E_{b,13}$ of the two-body bound state in the first and third components [5, 6].

The Hamiltonian in Eq. (1) describes an asymmetric three-component Fermi system: (i) The SOC only exists in the first two components, leading them to share the same chemical potential μ_{12} ; (ii) interaction occurs only between the first and third components. Such an asymmetric interaction can potentially give rise to pairing superfluidity between the first and third components.

Meanwhile, the asymmetric SOC modifies the momentum, energy, and population fraction of the first component. This manipulation is expected to have a significant impact on the possible pairing between the first and third components [52]. We apply mean-field theory to study the possible pairing. To proceed, we introduce the order parameter

$$\Delta_{13} = \frac{U_{13}}{S} \sum_{\mathbf{k}} \langle c_{\mathbf{Q}-\mathbf{k},1} c_{\mathbf{k},3} \rangle. \quad (6)$$

It is the pair between the first and third components with a finite center-of-mass momentum \mathbf{Q} , i.e., FF pairing. With this FF order parameter, the interacting H_I can be approximated as

$$H_I = \sum_{\mathbf{k}} \left(\Delta_{13}^* c_{\mathbf{Q}-\mathbf{k},1} c_{\mathbf{k},3} + \Delta_{13} c_{\mathbf{k},3}^\dagger c_{\mathbf{Q}-\mathbf{k},1}^\dagger \right) - \frac{S |\Delta_{13}|^2}{U_{13}}.$$

We further construct the Nambu basis $\psi_{\mathbf{Q}}(\mathbf{k}) = (c_{\mathbf{k},1}, c_{\mathbf{k},2}, c_{\mathbf{k},3}, c_{\mathbf{Q}-\mathbf{k},1}^\dagger, c_{\mathbf{Q}-\mathbf{k},2}^\dagger, c_{\mathbf{Q}-\mathbf{k},3}^\dagger)^T$. With the mean-field approximation in H_I , the total Hamiltonian in Eq. (1) can be expressed in the Nambu basis space as [16, 44, 52],

$$H = \frac{1}{2} \sum_{\mathbf{k}} \psi_{\mathbf{Q}}^\dagger(\mathbf{k}) M_{\mathbf{Q}}(\mathbf{k}) \psi_{\mathbf{Q}}(\mathbf{k}) + \frac{1}{2} \sum_{\mathbf{k}} (3\varepsilon_{\mathbf{Q}-\mathbf{k}} - 2\mu_{12} - \mu_3) - \frac{S |\Delta_{13}|^2}{U_{13}}. \quad (7)$$

Here, the Bogoliubov–de-Gennes (BdG) matrix is

$$M_{\mathbf{Q}}(\mathbf{k}) = \begin{pmatrix} H_0(\mathbf{k}) & \Delta \\ \Delta^\dagger & -H_0(\mathbf{Q}-\mathbf{k}) \end{pmatrix}, \quad (8)$$

with the matrix Δ being

$$\Delta = \begin{pmatrix} 0 & 0 & -\Delta_{13} \\ 0 & 0 & 0 \\ \Delta_{13} & 0 & 0 \end{pmatrix}. \quad (9)$$

From the Hamiltonian H in Eq. (7), we calculate the thermodynamic potential $\Omega = -k_B T \ln \text{Tr} e^{-H/(k_B T)}|_{T \rightarrow 0}$, here, k_B is the Boltzmann constant and T is the temperature. The calculated result becomes,

$$\Omega = - \frac{1}{2} \sum_{\mathbf{k}, n} E_{\mathbf{Q}}^{(n)}(\mathbf{k}) \Theta \left[E_{\mathbf{Q}}^{(n)}(\mathbf{k}) \right] + \frac{1}{2} \sum_{\mathbf{k}} (3\varepsilon_{\mathbf{Q}-\mathbf{k}} - 2\mu_{12} - \mu_3) + \sum_{\mathbf{k}} \frac{|\Delta_{13}|^2}{2\varepsilon_{\mathbf{k}} + E_{b,13}}, \quad (10)$$

where Θ is the Heaviside step function, and $E_{\mathbf{Q}}^{(n)}(\mathbf{k})$ with $n = 1 - 6$ are eigenvalues of the BdG matrix $M_{\mathbf{Q}}(\mathbf{k})$.

The thermodynamic potential plays a central role in this study. For given chemical potentials μ_{12} and μ_3 , the

ground state should correspond to the global minimum of the thermodynamic potential. We first locate this minimum and, from it, determine the pairing momentum \mathbf{Q} and the order parameter Δ_{13} . All results indicate that \mathbf{Q} is always along the \hat{k}_x direction whenever it is nonzero:

$$\mathbf{Q} = Q_x \hat{k}_x, \quad (11)$$

where Q_x denotes the magnitude of the pairing momentum along the \hat{k}_x direction. This is reasonable because SOC plays an important role in the formation of FF pairs and is present only along the \hat{k}_x direction. The asymmetric three-component system offers a fundamental opportunity to tune the population imbalance between the pairing components by varying the chemical potentials. In the following, we fix the spin-orbit-coupled chemical potential μ_{12} and vary μ_3 to investigate FF pairing. We identify different types of pairing, which can be characterized by Q_x and Δ_{13} . For convenience in numerical calculations, we adopt units of energy and momentum as $E_{k_F} = \hbar^2 k_F^2 / 2m$ and k_F , respectively, where k_F is a typical momentum scale.

III. FF PAIR FOR WEAK SOC

The SOC parameters include the spin-orbit coupling strength α and the Raman coupling strength h . Depending on whether α dominates or not, the system resides in either the weak or strong SOC regime, where the spin-orbit-coupled single-particle spectrum exhibits a dramatic difference.

We first study the weak SOC case. Figure 1(a) shows the single-particle dispersion of $H_0(\mathbf{k})$ in Eq. (2). The black line represents the energy band of the third component, while colorful lines correspond to the spin-orbit-coupled energy bands of the first and second components. The color scale in these lines denotes the population fraction, with red (blue) indicating dominance of the first (second) component. We fix the chemical potential $\mu_{12} = 1.1$ (green-dashed line), which intersects two spin-orbit-coupled bands and yields two states dominated by the first component. The state in the upper (lower) spin-orbit-coupled band is marked by the green open (solid) circle. Clearly, these two states have different Fermi surface sizes, with the lower-band state exhibiting a larger Fermi surface. Meanwhile, we choose the chemical potential μ_3 such that it produces two states (represented by purple solid and open circles) after intersecting the dispersion of the third component. These two states lie on the same Fermi surface. We anticipate that FF pairing occurs among these four labeled states.

Once the chemical potentials μ_{12} and μ_3 are given, we calculate the thermodynamic potential Ω in Eq. (10) for various values of parameters Q_x and Δ_{13} . Two representative results in the parameter space of (Δ_{13}, Q_x) for $\mu_3 = 0.1$ and $\mu_3 = 0.8$ are shown in Figs. 1(c) and 1(d), respectively. From the calculated Ω , we identify the locations of its minima, which are marked by red circles.

These minima correspond to the ground state of the system. In each minimum, if $\Delta_{13} = 0$, the ground state is in the normal phase (N); if $\Delta_{13} \neq 0$ and $Q_x \neq 0$, the ground state is in the FF pairing superfluid phase. We find that the FF pairs in Figs. 1(c) and 1(d) exhibit different behavior, and thus we designate them as FF1 and FF2 phases, respectively. Interestingly, for this asymmetric three-component system, there is no conventional superfluid phase characterized by $\Delta_{13} \neq 0$ and $Q_x = 0$ [52].

We fix the chemical potential $\mu_{12} = 1.1$ and vary μ_3 , then repeat the above calculation of the thermodynamic potential to determine the values of Δ_{13} and Q_x for the ground states. These values are plotted as functions of μ_3 in Fig. 1(b).

(1) When μ_3 is negative, the system is in the normal phase (N). In this regime, μ_3 does not intersect the energy band of the third component; consequently, the finite binding energy $E_{b,13}$ is insufficient to bind the first and third components together into pairs.

(2) As μ_3 increases and eventually intersects the band of the third component, the system enters the FF1 phase (pink-shaded region). This phase is characterized by a nonzero Δ_{13} and a very small positive Q_x [see the inset in Fig. 1(b)]. The emergence of such a small positive Q_x provides an important clue to the pairing mechanism. In the FF1 region, μ_3 cuts the energy band of the third component, generating a small Fermi surface. Meanwhile, the Fermi surface of the upper-band state [indicated by the green open circle in Fig. 1(a)] is also very small, in contrast to the larger Fermi surface of the lower-band state [green solid circle in Fig. 1(a)]. The comparable sizes of the Fermi surfaces of the upper-band state and the third-component state facilitate pairing between them and naturally lead to a very small pairing momentum. The order parameter Δ_{13} increases with μ_3 , as a higher μ_3 enhances the density of the third component.

(3) As μ_3 increases further, the system enters the FF2 phase [light-green-shaded region in Fig. 1(b)]. The phase transition between the FF1 and FF2 phases is first order. In the FF2 phase, the pairing momentum Q_x is no longer small, and both Q_x and Δ_{13} increase with μ_3 . In this regime, the Fermi surface of the lower-band state becomes comparable in size to that of the third component, facilitating pairing between them [see the two solid circles in Fig. 1(a)]. Moreover, the Fermi surface of the third component lies inside that of the lower-band state, which gives rise to a negative pairing momentum Q_x . As μ_3 continues to increase, the Fermi surface of the third component expands, causing the pairing momentum to become less negative.

We show that the FF1 (FF2) phase corresponds to the formation of pairs between the third component and the upper- (lower-) band spin-orbit-coupled state. By tuning μ_3 , a phase transition between these two phases can be induced. We emphasize that the order parameter Δ_{13} in the FF2 phase is always larger than that in the FF1 phase. This is because the Fermi surface of the lower-band state is larger than that of the upper-band state,

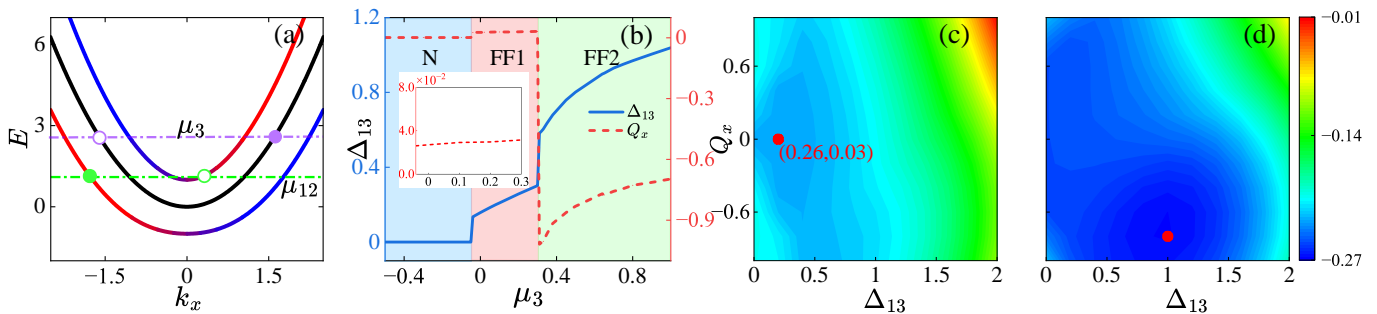


FIG. 1. FF pairs in an asymmetric three-component Fermi gas with weak SOC, $\alpha = 1$, $h = 1$, and $E_{b,13} = 0.5$. (a) Single-particle dispersion of $H_0(\mathbf{k})$ as a function of k_x for $k_y = 0$. The isolated energy band of the third component is shown by the black line. The spin-orbit-coupled energy bands of the first and second components are shown by the colored lines. The red (blue)-colored parts emphasize the dominant occupation of the first (second) component. The green-dashed horizontal line represents $\mu_{12} = 1.1$, which cuts through both the spin-orbit-coupled bands, generating an upper-band state (labeled by a green open circle) and a lower-band state (labeled by a green solid circle). The chemical potential μ_3 cuts through the third-component band, resulting in two states (labeled by purple open and solid circles). (b) Phase diagram showing the evolution of Δ_{13} (blue solid line) and Q_x (red-dashed line) of the ground states as functions of μ_3 . The diagram includes the normal phase (N, light blue region), the FF1 phase (light red region), and the FF2 phase (light green region). The inset shows a zoom-in of Q_x in the FF1 phase. (c) and (d) show the thermodynamic potential Ω in the parameter space of (Δ_{13}, Q_x) for $\mu_3 = 0.1$ and $\mu_3 = 0.8$, respectively. The global minimum of the thermodynamic potential is labeled by a red circle.

resulting in a higher density in the lower-band state. Reference [52] studied the same weak SOC case and reported results similar to ours. In the following, we investigate the strong SOC case, which goes beyond the study in Ref. [52], and identify the existence of a new type of FF pair.

IV. FF PAIR FOR STRONG SOC

The strong SOC gives rise to a double-well structure in the lower spin-orbit-coupled band, as shown in Fig. 2(a1). We find that the choice of μ_{12} has a significant effect on FF pairs.

A. μ_{12} cuts through both spin-orbit-coupled bands

We first study the case where μ_{12} cuts through both spin-orbit-coupled bands. As indicated by the green solid and open circles in Fig. 2(a1), this choice of μ_{12} yields two available states that are dominated by the first component [see the red-colored line]. In Fig. 2(a2), Q_x and Δ_{13} of the ground states are shown as functions of μ_3 . The phase diagram is similar to that in Fig. 1(b): The pink region corresponds to the FF1 phase, in which FF pairing occurs between the upper-band state (green open circle) and the third component; the FF2 phase (light-green region), on the other hand, corresponds to FF pairing between the lower-band state (green solid circle) and the third component.

B. μ_{12} lies within the spin-orbit-coupled gap

If μ_{12} is chosen to lie inside the spin-orbit-coupled gap, as shown in Fig. 2(b1), only one first-component-dominated state remains in the lower band (green solid circle). This state can bind with the third-component state (purple solid circle) to form an FF2 pair. Since no upper-band state is cut by μ_{12} , the FF1 pair cannot exist. The phase diagram presented in Fig. 2(b2) shows that increasing μ_3 leads to a first-order phase transition directly from the normal phase to the FF2 phase, without passing through the FF1 phase.

C. μ_{12} cuts through the double-well structure in the lower spin-orbit-coupled band

The results for the two choices of μ_{12} discussed above are very similar to those for the weak SOC case presented in the previous section. However, when μ_{12} is chosen to intersect the double-well structure in the lower spin-orbit-coupled band, no analogue exists in the weak SOC regime. This parameter configuration thus represents a unique feature of the strong SOC case.

Fig. 2(c1) shows that when μ_{12} intersects the double-well structure, two first-component-dominated states are generated, labeled by the green solid circle “a” and the green open circle “c”. Meanwhile, μ_3 gives rise to two possible states, marked by the purple open circle “b” and the purple solid circle “d”. The “a” and “d” states can form a pair with a finite net pairing momentum q_1 , as these two states have opposite group velocities. For the same reason, the “b” and “c” states can form a pair with a finite net pairing momentum q_2 . The combination of these two distinct pairs gives rise to a new FF state with

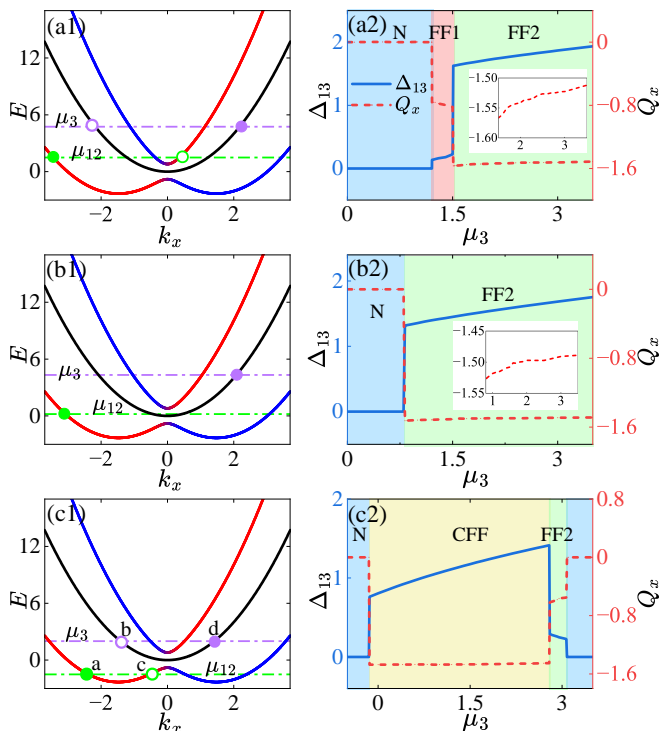


FIG. 2. FF pairs in an asymmetric three-component Fermi gas with strong SOC, $\alpha = 3$, $h = 0.8$, and $E_{b,13} = 0.5$. The left panels show the single-particle energy bands, and the right panels show the corresponding phase diagrams. (a1) and (a2) $\mu_{12} = 1.5$ cuts through both spin-orbit-coupled bands. (b1) and (b2) $\mu_{12} = 0.2$ lies within the spin-orbit coupling gap. The insets in (a2) and (b2) provide zoomed-in views of Q_x to illustrate its variation. (c1) and (c2) $\mu_{12} = -1.5$ cuts through the double-well structure within the lower spin-orbit-coupled band. The new composite FF phase, labeled “CFF”, is shown in the light yellow region.

a pairing momentum $Q_x = (q_1 + q_2)/2$ in order to minimize the energy. We name this new state the CFF state. The phase diagram shown in Fig. 2(c2) indicates that the CFF phase can exist over a wide range of μ_3 . A distinct feature of the CFF phase is that the pairing momentum Q_x remains constant ($Q_x = -1.47$ for the parameters in Fig. 2(c2)) throughout the entire region where it exists. We have checked other values of the chemical potential μ_{12} that cut through the double-well structure and found that the CFF phase consistently exhibits $Q_x = -1.47$. In the CFF phase, an increase in μ_3 causes the momenta k_x of the “b” and “d” states to expand symmetrically in opposite directions. Consequently, q_1 in the pair formed by the “a” and “d” states increases by an amount exactly equal to the decrease in q_2 in the pair formed by the “b” and “c” states. As a result, the average pairing momentum $Q_x = (q_1 + q_2)/2$ remains invariant as μ_3 varies.

We interpret the CFF phase as arising from a composite FF pair. The two third-component states, “b” and “d”, induced by μ_3 , form a composite third-component state with an average momentum of zero ($k_x = 0$). Mean-

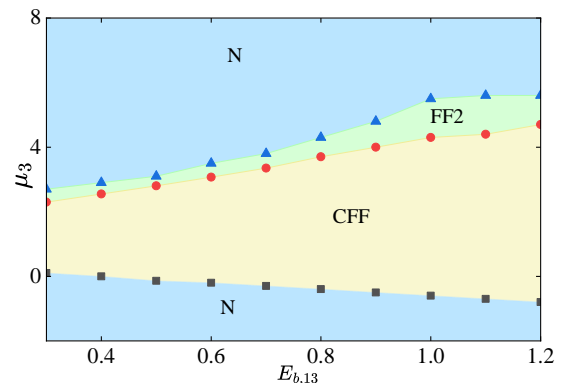


FIG. 3. Phase diagram in the $(E_{b,13}, \mu_3)$ plane. The parameters are the same as those in Fig. 2 with $\mu_{12} = -1.5$.

while, the two first-component-dominated states, “a” and “c”, generated by μ_{12} , form a composite first-component state whose average momentum corresponds to the location of the left minimum in the double-well structure. These two composite states then bind to form a composite FF pair, and consequently the pairing momentum becomes the left-minimum momentum of the lower spin-orbit-coupled band.

With this composite FF pair picture, we can readily understand why the pairing momentum Q_x in the CFF phase remains invariant under changes in μ_3 and μ_{12} . Variations in μ_3 and μ_{12} do not alter the average momenta of the composite third-component and first-component states, respectively. If we consider a negative strong SOC strength ($-\alpha$), the average momentum of the composite first-component state shifts to correspond to the right minimum of the lower spin-orbit-coupled band. Numerical calculations of the ground states confirm that the CFF phase can indeed exist, with the pairing momentum exactly equal to this right-minimum momentum.

Fig. 2(c2) shows a first-order phase transition from the CFF phase to the FF2 phase as μ_3 increases. In the FF2 phase, the pairing momentum q_1 in the FF pair formed by the “b” and “c” states becomes largely negative, rendering this FF pair energetically unfavorable. Consequently, the composite FF pair collapses, leaving only the FF pair formed by the “a” and “d” states. Compared to the CFF phase, the FF2 phase exists only in a narrow region of μ_3 . As μ_3 increases further, it is followed by the normal phase.

We emphasize that the CFF phase can exist over a very broad range of the binding energy $E_{b,13}$. A phase diagram in the $(E_{b,13}, \mu_3)$ plane is presented in Fig. 3. Interestingly, the region of the CFF phase along the μ_3 dimension expands as $E_{b,13}$ increases. The binding energy helps inhibit the collapse of the composite FF pairs. Meanwhile, the FF2 phase continues to exist throughout.

V. CONCLUSIONS

An asymmetric three-component Fermi gas provides an important platform for investigating exotic FF superfluids by combining SOC with population imbalance (via chemical potential mismatch). We systematically study the ground-state phase diagram of such an asymmetric three-component Fermi gas by finding the global minima of the thermodynamic potential. Strong SOC gives rise to a double-well structure in momentum space within the lower spin-orbit-coupled band. By choosing the chemical potential to intersect this double-well structure, we reveal a new composite FF superfluid. This composite FF superfluid exists over a wide range of parameters, and its pairing momentum remains invariant under changes in

the chemical potentials.

ACKNOWLEDGMENTS

This work is supported by the National Natural Science Foundation of China (NSFC) under Grants No.12374247 and No.11974235, by the Shanghai Municipal Science and Technology Major Project (Grant No. 2019SHZDZX01-ZX04), and the Shanghai Science and Technology Innovation Action Plan (Grant No. 24LZ1400800), as well as by the State Key Laboratory of Micro-nano Engineering Science (Grant No. MES202605).

-
- [1] I. Bloch, J. Dalibard, and W. Zwerger, Many-body physics with ultracold gases, *Rev. Mod. Phys.* **80**, 885 (2008).
 - [2] J. R. Schrieffer, *Theory of superconductivity* (CRC press, 1999).
 - [3] S. Giorgini, L. P. Pitaevskii, and S. Stringari, Theory of ultracold atomic Fermi gases, *Rev. Mod. Phys.* **80**, 1215 (2008).
 - [4] G. C. Strinati, P. Pieri, G. Röpke, P. Schuck, and M. Urban, The BCS-BEC crossover: From ultra-cold Fermi gases to nuclear systems, *Phys. Rep.* **738**, 1 (2018).
 - [5] M. Randeria, J.-M. Duan, and L.-Y. Shieh, Superconductivity in a two-dimensional Fermi gas: Evolution from Cooper pairing to Bose condensation, *Phys. Rev. B* **41**, 327 (1990).
 - [6] M. Marini, F. Pistolesi, and G. C. Strinati, Evolution from BCS superconductivity to Bose condensation: analytic results for the crossover in three dimensions, *Eur. Phys. J. B* **1**, 151 (1998).
 - [7] C. A. Regal, M. Greiner, and D. S. Jin, Observation of Resonance Condensation of Fermionic Atom Pairs, *Phys. Rev. Lett.* **92**, 040403 (2004).
 - [8] M. W. Zwierlein, C. A. Stan, C. H. Schunck, S. M. F. Raupach, A. J. Kerman, and W. Ketterle, Condensation of Pairs of Fermionic Atoms near a Feshbach Resonance, *Phys. Rev. Lett.* **92**, 120403 (2004).
 - [9] P. Fulde and R. A. Ferrell, Superconductivity in a Strong Spin-Exchange Field, *Phys. Rev.* **135**, A550 (1964).
 - [10] A. I. Larkin and Y. N. Ovchinnikov, Nonuniform state of superconductors, *Sov. Phys. JETP* **20**, 762 (1965).
 - [11] R. Casalbuoni and G. Nardulli, Inhomogeneous superconductivity in condensed matter and QCD, *Rev. Mod. Phys.* **76**, 263 (2004).
 - [12] L. Radzihovsky and D. E. Sheehy, Imbalanced Feshbach-resonant Fermi gases, *Rep. Prog. Phys.* **73**, 076501 (2010).
 - [13] W. Yi, W. Zhang, and X. Cui, Pairing superfluidity in spin-orbit coupled ultracold Fermi gases, *Sci. China Phys. Mech. Astron.* **58**, 1 (2015).
 - [14] Y. Xu and C. Zhang, Topological Fulde-Ferrell Superfluids of a Spin-Orbit Coupled Fermi Gas, *Int. J. Mod. Phys. B* **29**, 1530001 (2015).
 - [15] T. Paananen, J.-P. Martikainen, and P. Törmä, Pairing in a three-component Fermi gas, *Phys. Rev. A* **73**, 053606 (2006).
 - [16] T. N. De Silva, Three-component fermion pairing in two dimensions, *Phys. Rev. A* **80**, 013620 (2009).
 - [17] T. Ozawa and G. Baym, Population imbalance and pairing in the BCS-BEC crossover of three-component ultracold fermions, *Phys. Rev. A* **82**, 063615 (2010).
 - [18] D. E. Sheehy and L. Radzihovsky, BEC-BCS Crossover in “Magnetized” Feshbach-Resonantly Paired Superfluids, *Phys. Rev. Lett.* **96**, 060401 (2006).
 - [19] J. Zhang and H. Zhai, Pairing between atoms and molecules in a boson-fermion resonant mixture, *Phys. Rev. A* **72**, 041602 (2005).
 - [20] Y.-a. Liao, A. S. C. Rittner, T. Paprotta, W. Li, G. B. Partridge, R. G. Hulet, S. K. Baur, and E. J. Mueller, Spin-imbalance in a one-dimensional Fermi gas, *Nature* **467**, 567 (2010).
 - [21] M. M. Parish, F. M. Marchetti, A. Lamacraft, and B. D. Simons, Finite-temperature phase diagram of a polarized Fermi condensate, *Nat. Phys.* **3**, 124 (2007).
 - [22] M. W. Zwierlein, A. Schirotzek, C. H. Schunck, and W. Ketterle, Fermionic superfluidity with imbalanced spin populations, *Science* **311**, 492 (2006).
 - [23] G. B. Partridge, W. Li, R. I. Kamar, Y.-a. Liao, and R. G. Hulet, Pairing and phase separation in a polarized Fermi gas, *Science* **311**, 503 (2006).
 - [24] P. Wang, Z.-Q. Yu, Z. Fu, J. Miao, L. Huang, S. Chai, H. Zhai, and J. Zhang, Spin-Orbit Coupled Degenerate Fermi Gases, *Phys. Rev. Lett.* **109**, 095301 (2012).
 - [25] L. W. Cheuk, A. T. Sommer, Z. Hadzibabic, T. Yefsah, W. S. Bakr, and M. W. Zwierlein, Spin-Injection Spectroscopy of a Spin-Orbit Coupled Fermi Gas, *Phys. Rev. Lett.* **109**, 095302 (2012).
 - [26] Y.-J. Lin, K. Jiménez-García, and I. B. Spielman, Spin-orbit-coupled Bose-Einstein condensates, *Nature* **471**, 83 (2011).
 - [27] W. Zhang and W. Yi, Topological Fulde-Ferrell-Larkin-Ovchinnikov states in spin-orbit-coupled Fermi gases, *Nat. Commun.* **4**, 2711 (2013).
 - [28] C. Qu, Z. Zheng, M. Gong, Y. Xu, L. Mao, X. Zou, G. Guo, and C. Zhang, Topological superfluids with finite-momentum pairing and Majorana fermions, *Nat. Com-*

- mun. **4**, 2710 (2013).
- [29] Z. Zheng, M. Gong, X. Zou, C. Zhang, and G. Guo, Route to observable Fulde-Ferrell-Larkin-Ovchinnikov phases in three-dimensional spin-orbit-coupled degenerate Fermi gases, *Phys. Rev. A* **87**, 031602 (2013).
- [30] Z. Zheng, M. Gong, Y. Zhang, X. Zou, C. Zhang, and G. Guo, FFLO superfluids in 2D spin-orbit coupled Fermi gases, *Sci. Rep.* **4**, 6535 (2014).
- [31] J. Zhou, W. Zhang, and W. Yi, Topological superfluid in a trapped two-dimensional polarized Fermi gas with spin-orbit coupling, *Phys. Rev. A* **84**, 063603 (2011).
- [32] F. Wu, G.-C. Guo, W. Zhang, and W. Yi, Unconventional Fulde-Ferrell-Larkin-Ovchinnikov pairing states in a Fermi gas with spin-orbit coupling, *Phys. Rev. A* **88**, 043614 (2013).
- [33] C. Chen, Inhomogeneous Topological Superfluidity in One-Dimensional Spin-Orbit-Coupled Fermi Gases, *Phys. Rev. Lett.* **111**, 235302 (2013).
- [34] X.-J. Liu and H. Hu, Topological Fulde-Ferrell superfluid in spin-orbit-coupled atomic Fermi gases, *Phys. Rev. A* **88**, 023622 (2013).
- [35] Y. Xu, R.-L. Chu, and C. Zhang, Anisotropic Weyl Fermions from the Quasiparticle Excitation Spectrum of a 3D Fulde-Ferrell Superfluid, *Phys. Rev. Lett.* **112**, 136402 (2014).
- [36] Y. Cao, S.-H. Zou, X.-J. Liu, S. Yi, G.-L. Long, and H. Hu, Gapless Topological Fulde-Ferrell Superfluidity in Spin-Orbit Coupled Fermi Gases, *Phys. Rev. Lett.* **113**, 115302 (2014).
- [37] M. Iskin and A. L. Subasi, Topological superfluid phases of an atomic Fermi gas with in- and out-of-plane Zeeman fields and equal Rashba-Dresselhaus spin-orbit coupling, *Phys. Rev. A* **87**, 063627 (2013).
- [38] X.-F. Zhou, G.-C. Guo, W. Zhang, and W. Yi, Exotic pairing states in a Fermi gas with three-dimensional spin-orbit coupling, *Phys. Rev. A* **87**, 063606 (2013).
- [39] L. Dong, L. Jiang, and H. Pu, Fulde-Ferrell pairing instability in spin-orbit coupled Fermi gas, *New J. Phys.* **15**, 075014 (2013).
- [40] W. Yi and W. Zhang, Molecule and Polaron in a Highly Polarized Two-Dimensional Fermi Gas with Spin-Orbit Coupling, *Phys. Rev. Lett.* **109**, 140402 (2012).
- [41] Z. Zheng and Z. D. Wang, Cavity-induced Fulde-Ferrell-Larkin-Ovchinnikov superfluids of ultracold Fermi gases, *Phys. Rev. A* **101**, 023612 (2020).
- [42] L. Morales-Molina and F. Isaule, Resonance detuning mechanism for directing particle flow in ring lattices, *Phys. Rev. A* **110**, 053313 (2024).
- [43] J. Chen, H. Hu, and X. Gao, Three-component topological superfluid in one-dimensional Fermi gases with spin-orbit coupling, *Phys. Rev. A* **90**, 023619 (2014).
- [44] F. Qin, F. Wu, W. Zhang, W. Yi, and G.-C. Guo, Three-component Fulde-Ferrell superfluids in a two-dimensional Fermi gas with spin-orbit coupling, *Phys. Rev. A* **92**, 023604 (2015).
- [45] X. Qiu, X. Cui, and W. Yi, Universal trimers emerging from a spin-orbit-coupled Fermi sea, *Phys. Rev. A* **94**, 051604 (2016).
- [46] Z. Zheng, Y.-Q. Zhu, S. Zhang, S.-L. Zhu, and Z. D. Wang, Synthetic spin-orbit coupling for the multispin models in optical lattices, *Phys. Rev. A* **110**, 033327 (2024).
- [47] H. Hu, L. Jiang, X.-J. Liu, and H. Pu, Probing Anisotropic Superfluidity in Atomic Fermi Gases with Rashba Spin-Orbit Coupling, *Phys. Rev. Lett.* **107**, 195304 (2011).
- [48] L. He and X.-G. Huang, BCS-BEC Crossover in 2D Fermi Gases with Rashba Spin-Orbit Coupling, *Phys. Rev. Lett.* **108**, 145302 (2012).
- [49] Z.-Q. Yu and H. Zhai, Spin-Orbit Coupled Fermi Gases across a Feshbach Resonance, *Phys. Rev. Lett.* **107**, 195305 (2011).
- [50] M. Gong, S. Tewari, and C. Zhang, BCS-BEC Crossover and Topological Phase Transition in 3D Spin-Orbit Coupled Degenerate Fermi Gases, *Phys. Rev. Lett.* **107**, 195303 (2011).
- [51] G. Chen, M. Gong, and C. Zhang, BCS-BEC crossover in spin-orbit-coupled two-dimensional Fermi gases, *Phys. Rev. A* **85**, 013601 (2012).
- [52] L. Zhou, X. Cui, and W. Yi, Three-Component Ultracold Fermi Gases with Spin-Orbit Coupling, *Phys. Rev. Lett.* **112**, 195301 (2014).